Feasibility Study of the Use of Operational Amplifiers as Forward Gain Stages in Charge Preamplifiers and Shaping Filters for Radiation Detectors

A. Castoldi, *Member, IEEE*, C. Guazzoni, *Senior Member, IEEE*, and A. Naggi

***Abstract*— Different application fields require the development of charge preamplifiers to be coupled with dedicated radiation detectors. In view of fast prototyping and targeting a medium number of readout channels, there are several advantages to the use of operational amplifiers (OpAmps) for the forward gain stage of charge preamplifiers and shaping filters. In this article, we present the feasibility study, design, and qualification of an OpAmp-based, charge preamplifier suited to equip a smart rad-hard detection system for the diagnostics and tagging of radioactive ion beams (RIBs) at high intensities (10^6 pps or higher). This article illustrates the conception and design of the fast readout system and presents a detailed analysis and qualification of its performance.**

***Index Terms*— Charge preamplifiers, high speed electronics, operational amplifiers (OpAmps), particle tagging, radiation detector circuits.**

I. Introduction

SEVERAL application fields in radiation detection require the development of fast readout systems. We choose here a target application in radioactive ion beams (RIBs) diagnostics and tagging at high intensities (10^6 pps or higher). One of the hottest topics in nuclear physics is the investigation of the properties of nuclei sitting far from the stability line and being either neutron rich or proton rich. Such studies could pave the way for new paradigms in nuclear physics and allow the study of reactions of fundamental importance for the nucleosynthesis of elements in the universe [1], [2], [3]. Radioactive beams need dedicated facilities for their production. In the framework of the upgrade [4] of the facility at INFN-LNS to improve the available power of the produced beams of two orders of magnitude (ions from C to Ar, with an intensity up to 10 kW) [5], a novel FRAgment In-fight SEparator (FraISe) [6], [7], [8] will produce high-intensity RIBs. During the process, many nuclear species, mostly stable isotopes, are produced and the first magnetic dipole would produce high and potentially harmful doses of γ radiations and neutrons, despite the presence of adequate shielding for high radiation doses. Therefore, the power of the cyclotron is limited to about 2–3 kW for the production of radioactive beams. The production technique, by means of in-flight fragment separation, is not able to deliver a pure beam as the produced beam, the so-called cocktail beam, contains several stable and unstable isotopes that, in the case of the same mass over-charge ratio, cannot be separated magnetically. This calls for the full characterization of the beam components arriving on the target on an event-by-event basis, in order to off-line select the isotope of interest for the reaction under study. Such an identification procedure is called tagging. In order to guarantee the highest possible rate or purity at the end-user station, it is necessary to develop dedicated diagnostic instruments able to provide a complete description of the RIBs in real-time in terms of total yield, bidimensional profile, yield per isotope, energy distribution per isotope, and angular distribution. To this aim, we are conceiving a network of smart sensors, equipped with optimized frontend electronics, DAQ with data real-time management capabilities, and a dedicated software layer implementing artificial intelligence and machine learning techniques as a tool to improve the production, transport, and use of RIBs [9].

The detection system will be based on an array of detectors that have to withstand a particle rate ranging from 10^2 pps (in case of very exotic isotopes, extremely far from the stability valley) up to 10^7 pps, as typical for exotic isotopes near to the stability valley. As a consequence, segmentation and radiation hardness of the sensor are a must, leading to the choice of an array of SiC diodes [10], [11]. The RIB composition is obtained from the joint measurement of the energy loss (ΔE) of the ions passing through the detectors and the time of flight between two sensors or with respect to a given reference signal as the radio-frequency signal of a Cyclotron. For a full description of the detector refer to [9]. Fig. 1 [12] shows the 3-D CAD of the proposed detection system located in a DN160 spherical cross. The request for a compact and versatile system easy to be replaced suggested investigating the feasibility of the use of operational amplifiers (OpAmps) as forward gain stages in charge preamplifiers and shaping filters used as frontend electronics for radiation detectors for fast timing. The article is organized as follows. Section II illustrates the frontend design guidelines and computes the expected performance. Section III presents the designed front-end prototypes. Section IV shows

Manuscript received 28 March 2023; revised 27 April 2023; accepted 5 May 2023. Date of publication 1 June 2023; date of current version 18 July 2023. This work was supported in part by the Istituto Nazionale di Fisica Nucleare (INFN) within the framework of the CHIRONE Experiment and in part by the Ministero dell'Universita' e della Ricerca under Grant PRIN 2020, ANCHISE, Prot. n. 2020H8YFRE.

The authors are with the Dipartimento Elettronica, Informazione e Bioingegneria, Politecnico di Milano, 20133 Milan, Italy, and also with the Istituto Nazionale di Fisica Nucleare (INFN), Sezione di Milano, 20133 Milan, Italy (e-mail: Chiara.Guazzoni@mi.infn.it).

Color versions of one or more figures in this article are available at https://doi.org/10.1109/TNS.2023.3277223.

Digital Object Identifier 10.1109/TNS.2023.3277223

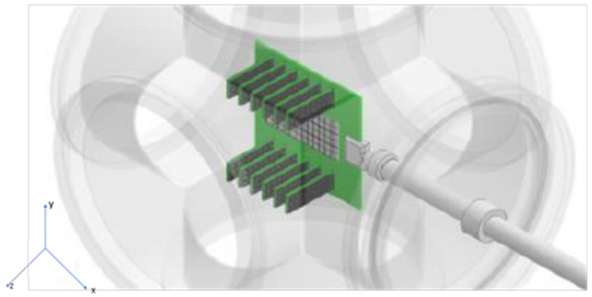

Fig. 1. Three dimensional CAD of the proposed detection system. Incoming beam is coming along the z-axis (negative direction) [12].

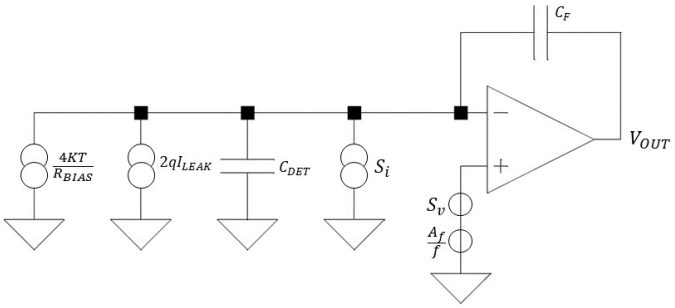

Fig. 2. Basic configuration of the frontend electronics in charge amplifier configuration. The main noise contributions are indicated by their equivalent noise generators.

the results of the experimental qualification, while Section V ends with the conclusions.

II. Frontend Design Guidelines and Expected Performance

The input dynamics depend on the energy loss in the detection layer. The large variety of produced exotic beams and beam intensities [9] requires a selectable gain configuration. The frontend electronics architecture is in charge preamplifier configuration. In order to fulfill the requirement of fast processing times to guarantee high-rate operation and excellent time resolution, the decay time constant of the preamplifier (for the return to 0) has to be fast, below 100 ns.

In order to evaluate the expected performance, we computed the achievable energy and time resolutions in an ideal configuration, schematically shown in Fig. 2. We consider an ideal Gaussian shaping amplifier, at the charge preamplifier output with a unipolar output. Ideally, a bipolar shaping is obtained as the first derivative of the unipolar Gaussian output.

The achievable energy resolution in terms of equivalent noise charge depends on the main noise sources of the frontend, highlighted in Fig. 2, mainly being the power spectral densities of the white series (S_v, due to the amplifier), white parallel ($S_i + 2q\ I_{\mathrm{LEAK}} + 4kT/R_{\mathrm{BIAS}}$) and $1/f$ series noises (A_f/f), and on the chosen shape (unipolar or bipolar), and on its duration, according to [9, eqs. (1) and (2)]. In addition, there is a dependence on the total virtual ground node capacitance. We considered a realistic value for the total capacitance, assumed equal to about 40 pF (21 pF detector capacitance at depletion for a 5 × 5 mm SiC diode 100 μm thick, plus 8 pF maximum stray capacitance due to bonding and pads and 11 pF input capacitance of the forward gain stage).

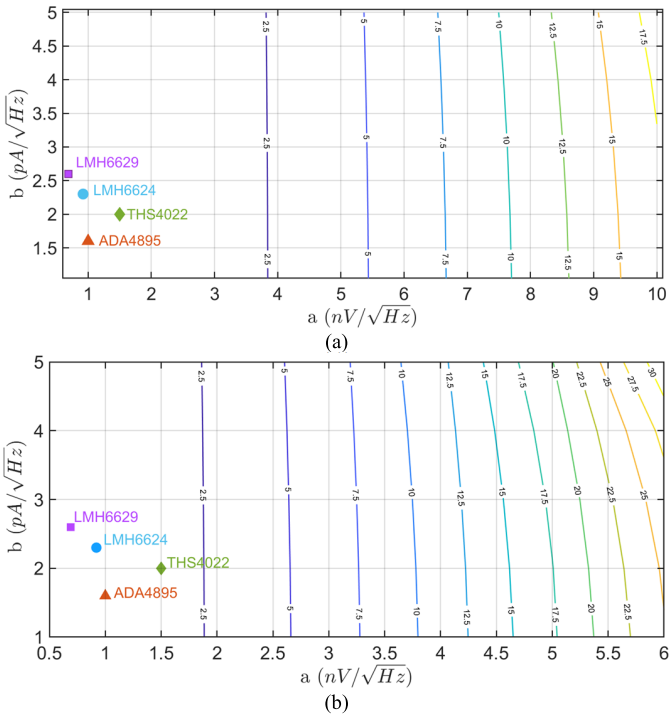

Fig. 3. Contour plot of the minimum shaping time (τ_{sh}) at (a) unipolar and (b) bipolar output (indicated in ns) able to guarantee an energy resolution below 100 keV r.m.s. as a function of the white series and white parallel noise power spectral densities of the frontend. Symbols represent the noise spectral densities of selected commercial OpAmps for the forward gain stage.

The charge preamplifier feedback capacitance depends on the required dynamic range and in the first design, intended for the detection of light ions, is set to 0.5 pF. The detector leakage current is fully negligible with respect to the input bias current of the OpAmp.

The following equation gives, in first approximation, the achievable time resolution r.m.s. (σ_t)

$$\sigma_t = \frac{\sqrt{\mathrm{ENC}(\tau_{\mathrm{sh\ bip}})^2}}{\left(\frac{\partial S_0}{\partial t}\Big|_{t=0}\right) Q_{\mathrm{loss}}} \tag{1}$$

where $(\partial S_0/\partial t)|_{t=0}$ is the slope at the zero crossing of the shaped output, obviously bipolar, while Q_{loss} is the charge deposited in each detection layer, $\tau_{\mathrm{shuni(bip)}}$ is the unipolar (bipolar) shaping time constant.

As a guideline for the design, we computed the achievable time and energy resolutions as a function of the noise parameters of the input parallel and series noise of the forward gain stage, assuming an ideal amplifying stage for the forward gain stage.

Fig. 3 shows the contour plot of the minimum shaping time (τ_{sh}) indicated in ns on the isarithms at the unipolar and bipolar output able to guarantee an energy resolution below 100 keV r.m.s. as a function of the white series and white parallel noise power spectral densities of the frontend charge preamplifier.

Fig. 4 shows the contour plot of the maximum shaping time (τ_{sh}) indicated in *ns* on the isarithms at the bipolar output required to guarantee a time resolution below 100 ps r.m.s. as a function of the white series and white parallel noise power spectral densities of the frontend electronics. Symbols

TABLE I
MAIN RELEVANT PARAMETERS OF THE CHOSEN OPAMPS

Parameter	THS4022	LMH6624	LMH6629	ADA4895
Power supply	±5 V to ±15 V	±2.25 to ±6.3	2.7 V to 5.5 V	±1.5 V to ±3V
Supply Current	6.7 – 7.8 mA	12 mA	15.5 mA	3 mA
GBWP	1.6 GHz	1.5 GHz	4 GHz	1.5 GHz
Stable at a gain of	10 (–9) or Greater	≥ 10	≥ 4 or ≥10 V/V	≥ 10
Slew Rate	470 V/µs	350 V/µs	1600 V/ µs	943 V/µs
Input Bias Current	3 µA ± 30 nA	13 µA - 60 nA	-15 µA ± 100 nA	-11 µA - 20 nA
Input Offset Voltage	±0.5 mV	±0.7 mV	±0.15 mV	-0.053 mV
Input Voltage Noise	1.5 nV/√Hz 10 nV/√Hz at 10 Hz	0.92 nV/√Hz 4.5 nV/√Hz at 100 Hz	0.69 nV/√Hz 1.3 nV/√Hz at 200 Hz	1 nV/√Hz 2 nV/√Hz at 10 Hz
Input Parallel Noise	2 pA/√Hz	2.3 pA/√Hz	2.6 pA/√Hz	1.6 pA/√Hz
Output Current	±100 mA	±100 mA	±250 mA	80 mA rms
Input capacitance	1.5pF	0.9 pF	1.7 pF	3 pF
Package	SOIC or MSOP	SOIC8 or SOT-23-5	WSON-8 and SOT-23-5	SOIC8 or SOT-23-5 MSOP10 dual

Table I summarizes the main relevant parameters of the proposed operational amplifiers.

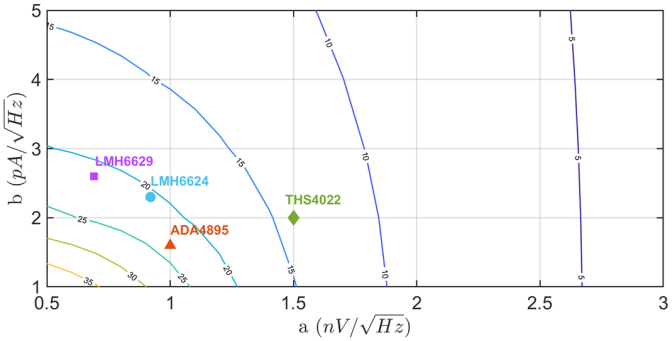

Fig. 4. Isarithms curves of the shaping time (τ_{sh},ns) at the bipolar output needed to provide a time resolution better than 100 ps r.m.s. as a function of the white series and white parallel noise power spectral densities of the frontend. Symbols represent the noise spectral densities of possible commercial OpAmps to be used for the forward gain stage.

represent the noise spectral densities of the same selected high-performance commercial OpAmps used in Fig. 3. Table I summarizes the main features of these proposed OpAmps. All selected OpAmps for the forward gain stage comfortably sit in the safe area for both timing and energy resolution.

III. DESIGNED FRONTEND PROTOTYPES

In order to compare experimentally the performance, we produced different prototypes, suitable to house the OpAmps listed in Table I that feature different footprints. Each board implements four readout channels, in order to allow the test of up to four detectors in parallel or a monolithic detector segmented into four detection cells. A Molex 50 03340 160 0.50 mm Pitch SlimStack Plug connects the preamplifier to the detector motherboard. A Molex Pico-Clasp connector provides the needed power lines.

The frontend output stage performs the conversion from single-ended to differential and buffers the long cables (up to about 10 m from the output of the OpAmp) capacitance that might cause instability. To perform a conversion from a single-ended signal to a differential one, fully differential amplifiers (FDAs) are the typical solution. To select the amplifier various considerations have been made. First, all

TABLE II
MAIN RELEVANT PARAMETERS OF THE CHOSEN FDAS

FDA	Supply current (mA)	GBWP (MHz)	SR (V/µs)	a (nV /√Hz)	b (pA /√Hz)	c (nV)
ADA4940	1.25	140	95	3.9	0.81	238
THS4551	1.37	135	220	3.4	0.5	79

Table II summarizes the main relevant parameters of the selected fully differential line drivers.

the noise sources added by the FDA, when referred back to the input, contribute to the series white noise power spectral density of the entire configuration, which, as discussed, plays a fundamental role in determining the performance of the system. In addition, a large common mode signal is expected at the FDA input, therefore good performance in terms of CMRR and matching of the two feedback networks are required. Last but not least, the closed-loop bandwidth of the FDA should be higher than the one of the CPA, which is higher than 20 MHz and to prevent reflections along the cables, impedance matching is mandatory, so a gain equal to (at least) two is required to compensate for the reduction of the signal amplitude. Table II lists the main features of the selected FDAs. If desired, this stage can insert additional poles along the signal path, thus merging the filtering and the output stage into a single circuit, with the minimization of both the occupied area and the required power budget. The differential output goes out through a Samtec HSEC8-113-01-S-DV-A-K-TR connector, mating with Samtec Eye-Speed Twinax cables, providing 100 ohm differential pair signal routing. A HIROSE U.FL-SMT-1(10) connector has been added at the output of each preamplifier to allow its evaluation at the single-ended version when not coupled to the output stage.

Fig. 5 shows the photograph of the different four-channel charge preamplifier boards that have been produced (only the JFET design is a single-channel version, for comparison purposes). All prototypes feature the same architecture and were designed under the same geometrical constraints and with the same layout, as shown in Fig. 6.

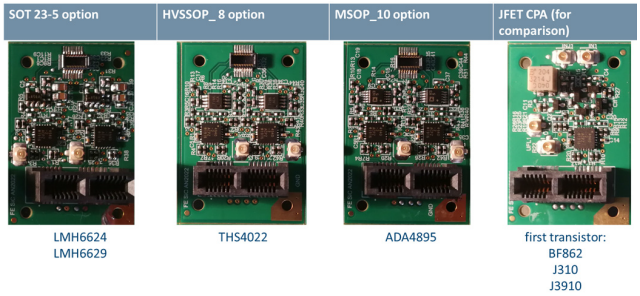

Fig. 5. Photograph of different four-channels charge preamplifier boards that have been produced (only the JFET design is a single-channel version).

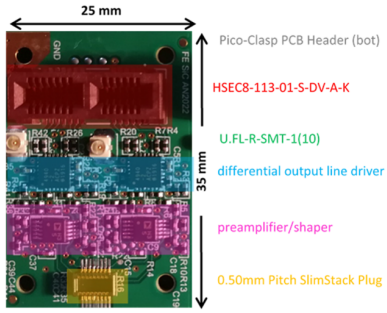

Fig. 6. Main components of the designed frontend based on OpAmps.

IV. Experimental Qualification

We performed a thorough qualification of the designed preamplifier prototypes, comparing the performance as a function of the chosen OpAmp. The availability of interchangeable boards allowed an easy comparison.

A. Output Waveforms

The feedback resistance is set to 47 kΩ and the feedback capacitance is 0.5 pF. The preamplifier output was directly digitized by a 5 GS/s oscilloscope with no bandwidth limitation for waveform acquisition. We acquired also several waveforms at the differential output. Fig. 7 shows the measured output waveforms (raw data) in the case of two different OpAmps. We observed no slew rate limitation over the full signal dynamics even at *0 pF* detector capacitance.

B. Impact of the Detector Capacitance and Measured Rise Time

We measured the rise time (10%–90%) as a function of the input capacitance. The input pulse comes from the Agilent 33250A Function/Arbitrary Waveform Generator featuring a 3.8 ns input signal rise time. As shown in Fig. 8, the slope of the linear fit ranges from 0.14 ns/pF for the ADA4895 to 0.19 ns/pF for the LMH6624. The input signal is depositing about 20 MeV silicon equivalent and the rise time is below 15 ns up to 50 pF additional input capacitance.

C. Integral Non-Linearity

The measured integral-non-linearity (INL)—computed as the maximum deviation from the linear fit up to the considered amplitude—is better than 0.6% up to 50 MeV deposited energy (silicon equivalent), showing a negligible impact on the

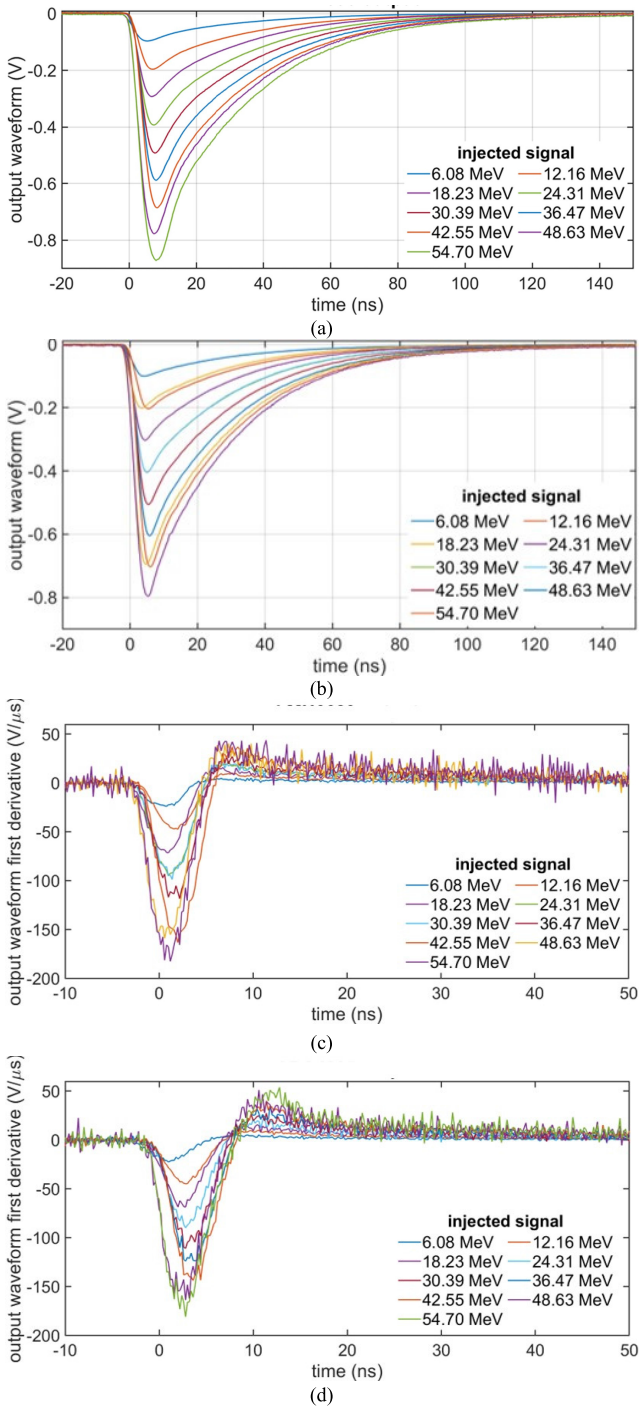

Fig. 7. Measured output waveform (raw data) in the case of two different OpAmps. (a) ADA4895. (b) LMH6624 and their time derivative showing no slew rate limitation. (c) ADA4895. (d) LMH6624.

detector capacitance. A much better INL, below 0.25% was measured in the case of the ADA4895, as shown in Fig. 9.

D. Fully Differential Amplifiers Output

We qualified the output response of the FDAs output as a function of the differential pair cable length. No one of the six evaluated configurations shows SR distortion. Fig. 10 shows the measured output waveforms for two different cable lengths (5 cm and 5 m) and for two different amplitudes of the injected signal in the case of the ADA4895 OpAmp used for

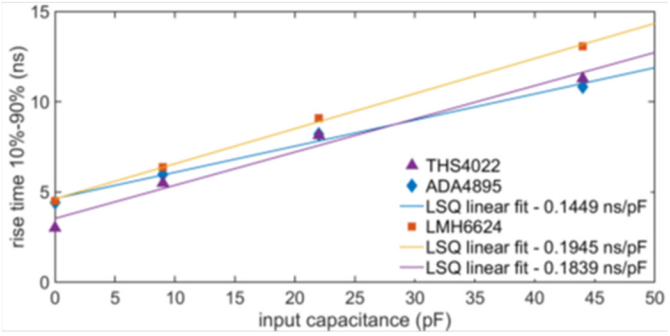

Fig. 8. Measured rise time as a function of the input capacitance, for three of the selected OpAmps. The deposited energy (silicon equivalent) is 20 MeV.

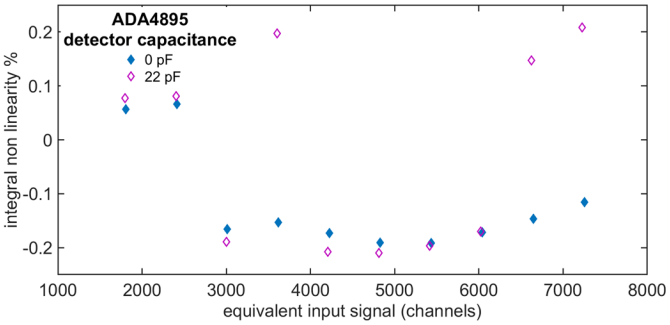

Fig. 9. Measured integral non-linearity as a function of the input signal amplitude, equivalent to a maximum signal of 50 MeV, in the case of the ADA4895 OpAmp, for two values of the total capacitance at the virtual ground.

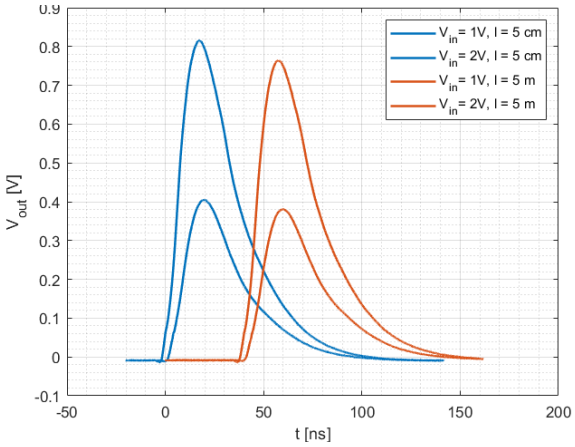

Fig. 10. Measured output waveforms at the fully differential output for two different cables lengths (5 cm and 5 m) and for two different amplitudes of the injected signal in the case of the ADA4895 OpAmp used for the forward stage and of the THS4552 FDA.

the forward stage and of the THS4552 FDA. The 5 m cable introduces a filtering action that results in all the cases in a reduction of the pulse peak amplitude of about 0.94 and a slight broadening of the pulse as expected. No instability or peaking is observed. Despite the THS4552 introducing a distortion of the slope of the pulse when it overcomes a threshold around 40–50 V/μs, this has no impact on the integral non-linearity of the configuration, as shown in Fig. 9.

V. Conclusion

In this article, we showed that fast preamplifier and shaping filters based on OpAmps are feasible, paving the way for a much cheaper and more versatile alternative with respect to ASICs and more compact with respect to transistor solutions. We selected suitable OpAmps some of them are low power and with compact footprints available also as dual OpAmps to save space if needed. We designed and produced the first prototypes in view of the construction of a smart rad-hard fast detection system. Their performance was experimentally assessed in the lab. We measured fast rise times below 15 ns for all experimented capacitive loads and down to below 1 ns. The measured INL keeps below 0.6% up to 50 MeV input signal for all the designed configurations. A much better INL is obtained in the case of the ADA4895 combined with the THS4552 with the additional advantage of the lowest power budget.

The LMH6629 built-in SiGe technology is compatible with low-temperature operation as required, for example, for the readout of systems for dark matter search [13].

We coupled the front end with a SiC detector prototype to assess the energy resolution and actual rise time. Preliminary measurements were carried out with a mixed nuclei alpha source placed very close to the detector in the air. The measured electronics noise is below 45 keV rms.

We will evaluate the impact of the detector segmentation on the achievable performance, in view of a detailed on-beam qualification with stable and radioactive beams and of the development of the front end for the full-scale detector.

References

[1] K. Hagino, E. M. Henley, and S. D. Ellis, *100 Years of Subatomic Physics*, vol. 231. Singapore: World Scientific, Singapore, 2013.

[2] I. Tanihata, "Nuclear structure studies from reaction induced by radioactive nuclear beams," *Prog. Part. Nucl. Phys.*, vol. 35, pp. 505–573, Jan. 1995.

[3] N. Alamanos, C. Bertulani, A. Bonaccorso, A. Bracco, D. M. Brink, and G. Casini, "Rewriting nuclear physics textbooks: 30 years with radioactive ion beam physics," *Eur. Phys. J. Plus*, vol. 132, no. 1, pp. 1–10, Jan. 2017.

[4] *INFN-LNS (POTenziamento dei Laboratori Nazionali del Sud—POTLNS)*. Accessed: Dec. 6, 2022. [Online]. Available: https://potlns.lns.infn.it/it/

[5] F. Risitano, "Simulation study of radioactive ion beams production at FRAISE (INFN-LNS)," *Il Nuovo Cimento C*, vol. 45, no. 4, pp. 1–10, 2022, doi: 10.1393/ncc/i2022-22068-9.

[6] P. Russotto et al., "Status and perspectives of the INFN-LNS in-flight fragment separator," *J. Phys., Conf. Ser.*, vol. 1014, May 2018, Art. no. 012016.

[7] A. D. Russo, L. Calabretta, G. Cardella, and P. Russotto, "Preliminary design of the new fragment in-flight separator (FRAISE)," *Nucl. Instrum. Methods Phys. Res. B, Beam Interact. Mater. At.*, vol. 463, pp. 418–420, Jan. 2020.

[8] N. S. Martorana, "Status of the FraISe facility and diagnostics system," *Il Nuovo Cimento C*, vol. 44, no. 1, pp. 1–10, 2021, doi: 10.1393/ncc/i2021-21001-2.

[9] C. Altana et al., "Feasibility study of a smart rad-hard fast detection system for radioactive ion beam tagging and diagnostics," in *Proc. IEEE Nucl. Sci. Symp. Med. Imag. Conf. (NSS/MIC)*, Oct. 2021, pp. 1–4.

[10] S. Tudisco et al., "SiCILIA—Silicon carbide detectors for intense luminosity investigations and applications," *Sensors*, vol. 18, no. 7, pp. 1–16, 2018.

[11] J. M. Rafí et al., "Electron, neutron, and proton irradiation effects on SiC radiation detectors," *IEEE Trans. Nucl. Sci.*, vol. 67, no. 12, pp. 2481–2489, Dec. 2020, doi: 10.1109/TNS.2020.3029730.

[12] L. A. Sanchez, private communication, Jun. 2022.

[13] A. Zani et al., "The ASTAROTH project: Enhanced low-energy sensitivity to dark matter annual modulation," *J. Phys., Conf. Ser.*, vol. 2156, no. 1, pp. 1–5, 2021, doi: 10.1088/1742-6596/2156/1/012060.

Open Access funding provided by 'Politecnico di Milano' within the CRUI CARE Agreement